

## Article

# Programmed Aptamer Screening, Characterization, and Rapid Detection for $\alpha$ -Conotoxin MI

Han Guo <sup>†</sup>, Bowen Deng <sup>†</sup>, Luming Zhao <sup>†</sup>, Yun Gao, Xiaojuan Zhang , Chengfang Yang, Bin Zou, Han Chen, Mingjuan Sun, Lianghua Wang <sup>\*</sup> and Binghua Jiao <sup>\*</sup>

Department of Biochemistry and Molecular Biology, College of Basic Medical Sciences, Naval Medical University, Shanghai 200433, China

<sup>\*</sup> Correspondence: lhwang@smmu.edu.cn (L.W.); bhjiao@smmu.edu.cn (B.J.)

<sup>†</sup> These authors contributed equally to this work and shared the first authorship.

**Abstract:** Conotoxins (CTXs) are a variety of mixed polypeptide toxins, among which  $\alpha$ -conotoxin MI (CTX-MI) is the most toxic. Serious toxic symptoms, a lack of counteracting drugs, and cumbersome detection processes have made CTX-MI a hidden danger for humans. One of the obstacles to resolving this problem is the absence of specific recognition elements. Aptamers have shown great advantages in the fields of molecule detection, drug development, etc. In this study, we screened and characterized aptamers for CTX-MI through a programmed process. MBMI-01c, the isolated aptamer, showed great affinity, with an affinity constant ( $K_D$ ) of 0.524  $\mu$ M, and it formed an antiparallel G-quadruplet (GQ) structure for the specific recognition of CTX-MI. Additionally, an aptasensor based on the biolayer interferometry (BLI) platform was developed and displayed high precision, specificity, and repeatability with a limit of detection (LOD) of 0.26  $\mu$ M. This aptasensor provides a potential tool for the rapid detection of CTX-MI in 10 min. The aptamer can be further developed for the enrichment, detoxification, and biological studies of CTX-MI. Additionally, the programmed process is applicable to screening and characterizing aptamers for other CTXs.



**Citation:** Guo, H.; Deng, B.; Zhao, L.; Gao, Y.; Zhang, X.; Yang, C.; Zou, B.; Chen, H.; Sun, M.; Wang, L.; et al. Programmed Aptamer Screening, Characterization, and Rapid Detection for  $\alpha$ -Conotoxin MI. *Toxins* **2022**, *14*, 706. <https://doi.org/10.3390/toxins14100706>

Received: 16 September 2022

Accepted: 11 October 2022

Published: 14 October 2022

**Publisher's Note:** MDPI stays neutral with regard to jurisdictional claims in published maps and institutional affiliations.



**Copyright:** © 2022 by the authors. Licensee MDPI, Basel, Switzerland. This article is an open access article distributed under the terms and conditions of the Creative Commons Attribution (CC BY) license (<https://creativecommons.org/licenses/by/4.0/>).

**Keywords:** alpha-conotoxin MI (CTX-MI); magnetic beads SELEX (MB-SELEX); high-throughput sequencing (HTS); aptamer; computer simulation; aptasensor

**Key Contribution:** (1) The aptamers for CTX-MI were screened by HT-MB-SELEX (MB-SELEX associated with HTS analysis). (2) The interaction mode and affinity parameters were determined by affinity detection combined with computer simulation. (3) A BLI-based aptasensor was developed for the rapid detection of CTX-MI.

## 1. Introduction

*Conus* species are carnivorous gastropods living in tropical and subtropical oceans [1]. Their venom ducts and poison glands secrete varieties of toxic polypeptides during predation and defense, which are called conotoxins (CTXs) [2]. Enormous gene families, abundant cysteines, and various post-translational modifications contribute to the diversity of CTXs [3,4]. According to statistics, the number of different sequences of CTXs has far exceeded 500,000 [3]. On the basis of signal peptides and disulfide bond skeletons, CTXs are divided into 26 superfamilies, which are represented by capital English letters; each superfamily is divided into several families based on the pharmacological targets, which are represented by lowercase Greek letters [2,5].

As a class of neurotoxins, CTXs act on a variety of ion channels and receptors throughout the nervous system, such as acetylcholine receptors and voltage-gated Na<sup>+</sup> channels, with high selectivity and potency [6]. The sting of cone snails can cause paralysis, dizziness, convulsion, respiratory failure, or even death [2,7]. Dating back to the 1960s, more than 300 poisonings, including 30 deaths, have been reported [6,8,9]. Alpha-conotoxin MI (CTX-MI), which was first

isolated from *Conus magus*, is considered as the most venomous species [10]. CTX-MI is a short peptide of 14 amino acids (GRCCHPACGKKNYS-C-NH<sub>2</sub>), which forms two disulfide bonds (Cys3-Cys8 and Cys1-Cys14) and selectively inhibits muscular acetylcholine receptors [11]. Due to a lack of clinical therapy and the unknown curative effect of antitoxic serums, the robust virulence of CTX-MI creates difficulties for prevention and clinical treatment [12]. In addition, the detection methods of CTX-MI rely on chromatography and mass spectrometry (MS) [13]. These methods are generally sensitive and precise. Nevertheless, the costly equipment, laborious sample purification, complex operation processes, and long testing time create barriers to their extensive applications [14]. The absence of specific recognition elements has been an obstacle to rapid detection and targeted therapy. As CTX-MI is a micro-molecular polypeptide with antigenicity but not immunogenicity, it is incapable of obtaining corresponding antibodies directly by immunizing animals. This deficiency of antibodies prompted us to screen novel recognition elements.

Aptamers, which are called “chemical antibodies”, are short single-strand DNA or RNA oligonucleotides with stable and unique three-dimensional (3D) structures [15]. For nearly one decade, multiple aptamers for small molecules have been successively screened [16,17]. These aptamers specifically tether targets with high affinity, suggesting that aptamers can be used as recognition elements for detection, detoxification, and biological research. Aptamers are usually screened by an *in vitro* approach called the systematic evolution of ligands by exponential enrichment (SELEX), which can exponentially enrich target-specific oligonucleotides from random libraries through rounds of screening and PCR amplification [18,19]. Aptamers have almost all the advantages of antibodies. More importantly, aptamers have unique features, including reproducibility, high thermal stability, low immunogenicity and toxicity, a lower cost of production, and permissible modification [16]. Hence, aptamers are expected to be applied in the detection, drug modification, and neurobiological research of CTX-MI.

In this study, we programmed screened, and characterized the specific and high-affinity aptamer for CTX-MI and verified its potential applications in rapid detection. The process was divided into four steps. (1) Candidate aptamers were enriched and isolated by magnetic beads SELEX (MB-SELEX). (2) Sequence diversity and the enrichment of candidate aptamers were analyzed using high-throughput sequencing (HTS) analysis. According to the HTS data, a total of 98 alternative sequences were screened. (3) The affinity and specificity of aptamers were determined by a biolayer interferometry (BLI) assay. Among these candidate aptamers, MBMI-01 had the highest affinity and specificity. Subsequently, the shorter aptamer, MBMI-01c, was obtained by removing the fixed regions. (4) The interaction mechanism was studied using computer simulation, which consisted of the 3D-structure prediction of the aptamer, molecular docking, and molecular dynamics (MD) simulation. The results revealed that MBMI-01c formed an antiparallel G-quadruplet (GQ) structure, and CTX-MI was tightly bound in the groove of the GQ structure by four hydrogen bonds. Additionally, a BLI-based aptasensor was developed and applied to CTX-MI detection in tap water. The aptasensor showed the potential for the rapid detection of CTX-MI in a concentration of 1–50  $\mu$ M with good precision and reproducibility.

## 2. Results and Discussion

### 2.1. The Isolation of Aptamers for CTX-MI

MB-SELEX included positive selection and counter selection (Figure 1A), and the counter selection was an optional step to remove the nonspecific adsorption to MBs or analogue  $\alpha$ -conotoxin GI (CTX-GI). To improve the enrichment of the dominant sequences, the screening pressure was increased by reducing the amount of the CTX-MI coated MBs (CTX-MI-MBs), reducing the incubation time, and increasing the washing time after incubation. The recovery ratio was significantly decreased at pressurized rounds (odd rounds), which proved that the sequences with weaker affinity were effectively removed (Figure 1B). Counter selection was introduced at round 7; blank MBs and CTX-GI-coated MBs (CTX-GI-MBs) were used for rounds 7–9 and 10–12, respectively. The counter selection

was effective, as the counter recovery ratios greatly decreased (Figure 1B). After 11 rounds of selection, the recovery ratio reached a plateau at 1.06% and showed no significant increase at round 12 (Figure 1B); hence, the screening process was terminated.

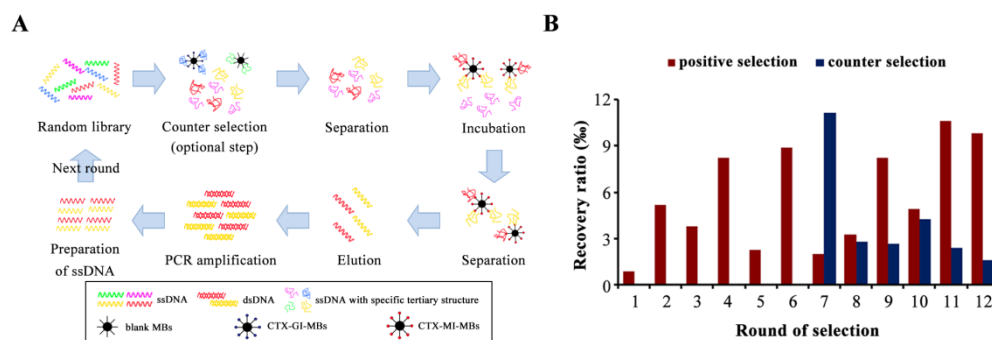


**Figure 1.** Aptamer selection in vitro. (A) The workflow of the magnetic beads SELEX (MB-SELEX). (B) The recovery ratio of ssDNA in the MB-SELEX. The recovery rate represents the ratio of the amount of ssDNA eluted from the magnetic beads to the amount of the ssDNA input in this round.

## 2.2. The Selection of Candidate Aptamers

Generally, the proportion of high-affinity aptamers presents a prominent preponderance after screening and PCR amplification. Therefore, compared with random clone sequencing in most previous reports [20–22], the HTS analysis reflects the enrichment of the dominant sequences and the variation in the sequence diversity more intuitively [23], which is more conducive to acquiring prominent aptamers. The libraries of rounds 2, 4, 6, 9, and 12 were chosen for HTS analysis. Rounds 2, 4, and 6 were the enriched rounds following the pressured rounds. Round 9 was the end of the blank counter selection, and round 12 was chosen as the last round.

A total of 138,149 unique sequences were detected. The pool of round 2 was highly diverse, containing 92.1% of unique sequences. With the increase in screening pressure, the sequence diversity was significantly decreased to 36.5% in round 12, which indicated the elimination of weak-affinity sequences (Figure 2A). Next, we retrieved the sequences with a frequency greater than 0.1% in round 12 as the prominent ssDNA (a total of 98 sequences). The percentage of prominent sequences increased from 6.9% (round 2) to 60.1% (round 12) (Figure 2B), indicating that the dominant sequences were amplified and enriched gradually with each round. An 18.2% reduction in sequence diversity and a 21.5% increase in the frequency of prominent aptamers were analyzed, although the condition of the positive selection in rounds 10–12 was the same as in round 9, demonstrating that the nonspecific aptamers were effectively eliminated (Figure 2A,B). The evolution of the 10 most enriched sequences is shown in Figure 2C, and the detailed information on the top 10 sequences is shown in Table S2. The highest-enriched sequence (MBMI-01) accounted for a frequency of 10.9% in round 12, and these 10 sequences showed a trend of enrichment, which also indicated the conditions were favorable for the enrichment of candidate ssDNA.

Subsequently, multiple sequence alignment was performed using Clustal X 2.1, and the neighbor-joining tree (N-J tree) was constructed by MEGA 7 (Figure S2). These 98 sequences were grouped into four families (I–IV) based on the N-J tree. The homologous sequences showed a wide range of conserved regions, which were probably related to the recognition of the target. Free energy was predicted using the Mfold web server (<http://www.unafold.org/mfold/applications/dna-folding-form.php>) (accessed on 15 September 2021); then, the aptamers with a higher frequency and lower free energy were chosen (Table S3).

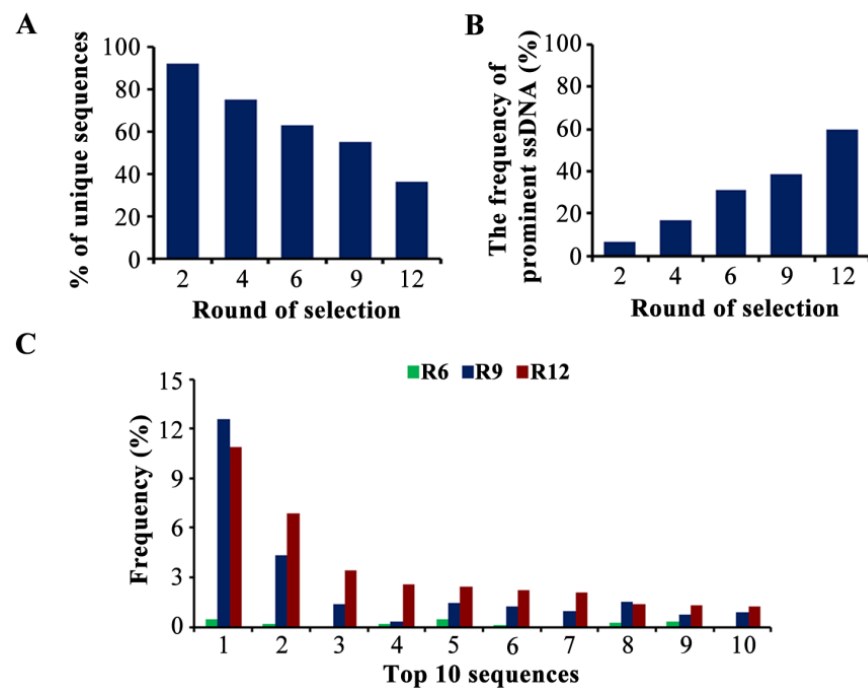


**Figure 2.** The analysis of the high-throughput sequencing (HTS) data. (A) The sequence diversity in each pool. The ordinate represents the number of unique sequences in each pool as a percentage of the total number of unique sequences. (B) The frequency of the prominent ssDNA in each pool. The ordinate represents the reads of the prominent ssDNA as a percentage of the total reads in each pool. (C) The frequency of the top 10 sequences. The ordinate represents the reads of each sequence as a percentage of the total reads in each pool.

### 2.3. The Determination of Affinity and Specificity

The affinity between the candidate aptamers and marine toxins was detected by BLI assay. Firstly, 10  $\mu\text{M}$  of CTX-MI was used for preliminary affinity detection. The results are shown in Table S4. Nine sequences (marked in red) had an affinity with CTX-MI with constant ( $K_D$ ) values ranging from 0.26 to 21.2  $\mu\text{M}$ . MBMI-01, MBMI-02, and MBMI-92 showed a relatively high affinity and response value in each family. The 10-bp complementary base pairs in the fixed regions could reduce the cross-linking between chains and promote the independent fold of random regions. Previous reports also showed the negligible contribution of fixed regions to the aptamer-target interaction [22]. Therefore, new aptamers (named MBMI-01c, MBMI-02c, and MBMI-92c) were resynthesized without the fixed regions; no significant change in the  $K_D$  values and a slight increase in response values were detected (Table S4). MBMI-01c, which had the highest response (0.2317 nm) and lowest  $K_D$  value (0.87  $\mu\text{M}$ ), was chosen for further determination.

Thereafter, CTX-MI with a series of concentration gradients (1.25, 2.5, 5, 10, and 20  $\mu\text{M}$ ) was used to accurately determine the affinity of MBMI-01c; and the  $K_D$  value was 0.524  $\mu\text{M}$  (Figure 3A). Specificity detection was conducted along with CTX-GI, domoic acid (DA), okadaic acid (OA), saxitoxin (STX), and tetrodotoxin (TTX), and the final concentration of each toxin was 10  $\mu\text{M}$ . CTX-GI is the analogue of CTX-MI, which is considered as the second most toxic CTX [24]. The DA, OA, STX, and TTX are the typical detection indexes of marine toxins. As shown in Figure 3B, high response values with no significant difference were monitored when CTX-MI or the mixture of the aforesaid six toxins were added, while there was almost no response in other groups, suggesting that MBMI-01c was bound to CTX-MI with specific high affinity.

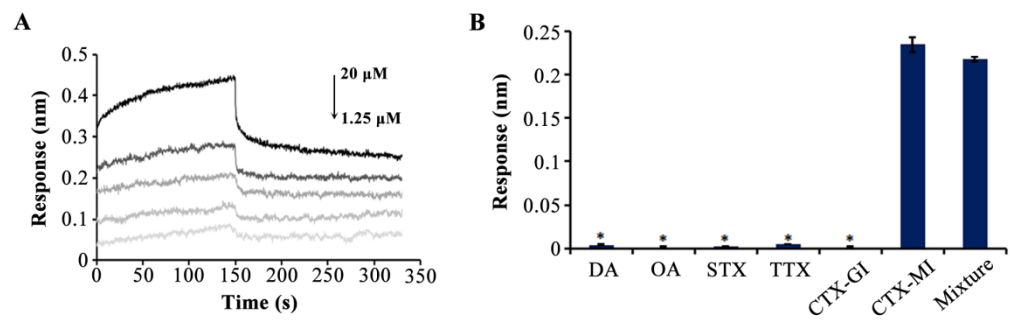


**Figure 3.** The affinity and specificity of MBMI-01c. **(A)** Association and dissociation curves after the addition of  $\alpha$ -conotoxin MI (CTX-MI) (the concentrations of CTX-MI corresponding to the five curves were 1.25, 2.5, 5, 10, and 20  $\mu\text{M}$  from bottom to top). The association step and dissociation step were 0–150 s and 150–300 s, respectively. **(B)** The response value for each target (10  $\mu\text{M}$ ). The target in the mixture group was the mixture of these six toxins (10  $\mu\text{M}$ ). Error bar represents the standard deviations. \*  $p < 0.05$  vs. CTX-MI group. All response values were detected by the BLI assay.

#### 2.4. The Interaction Mechanism between MBMI-01c and CTX-MI

Based on computer simulation, the 3D structure of the MBMI-01c and the interaction mechanism between MBMI-01c and CTX-MI were simulated. MBMI-01c had the basic body to form GQ, which might be the core structure combined with CTX-MI. To build the 3D model of MBMI-01c, we first identified the composition bases of the G-tetrads by quadruplex forming G-rich sequences (QGRS) prediction. There were four possible QGRS sequences (named A to D) with the highest G-scores of 19 (Table S5). After extending the non-GQ-core segments, we obtained nine candidate full-length models for each QGRS sequence named Q1 to Q5 and Q14 to Q17 (Figure S3). A temperature-dependent MD (TdMD) simulation was further carried out, and AQ1 (the Q1 model of structure A) proved to be the most stable model with the slightest root mean square deviation (RMSD) fluctuation (Figures S4–S6). We also mutated guanines to cytosines in MBMI-01c to preserve particular GQ structures, and the mutational sequences were named  $M_1$  to  $M_3$  (Tables S6 and S7). The invariant response value and  $K_D$  value were only detected in  $M_2$ , which only formed structure A with the highest G-scores (Table S6). Therefore, structure A was the primary structure to interact with CTX-MI compared with structures B, C, and D. Additionally, reduced affinity was detected in  $M_3$ , which perhaps related to the formation of the dominant structure E (Tables S6 and S7). Thus, AQ1 conformation at the end of the constant-temperature phase was employed as the native model (Figure 4A). MBMI-01c formed an antiparallel GQ with two G-planes (G4-G11-G26-G17 and G5-G10-G18-G25), which were connected by a  $\pi$  bond (Figures 4A,B and S3).

Thereafter, the interaction mechanism between MBMI-01c and CTX-MI was revealed using molecular docking. The  $E_{\text{total}}$ ,  $E_{\text{shape}}$ , and  $E_{\text{force}}$  are the main parameters for evaluating binding capacity.  $E_{\text{total}}$  and  $E_{\text{shape}}$  are inversely proportional to the hydrogen bonding energy and the spatial matching degree, respectively, while the lower  $E_{\text{force}}$  indicates the smaller mutual exclusion. As shown in Table 1, CTX-MI was evaluated as the tightest ligand with the lowest  $E_{\text{total}}$  value (−531.44 kcal/mol) and  $E_{\text{shape}}$  value (−531.44 kcal/mol) compared with other toxins. As shown in Figure 4C, CTX-MI was bound to the groove at the bottom of the GQ structure with hydrogen bonds. The T3, G4, C13, and T37 in MBMI-01c formed hydrogen bonds with the Gly1, Pro6, Cys4, and Lys10 in CTX-MI, respectively, and the H-bond distances were 2.7, 2.4, 2.7, and 1.9 Å, respectively (Figure 4C). The interaction between the G4 and Pro6 also provided a stable binding site at the top of GQ. Thus, CTX-MI was firmly adsorbed by the two G-planes and fixed in the groove. Conversely, hydrogen bonds were only observed between one of the G-planes and other toxins, even though more were formed with CTX-GI or STX, which led to lower spatial matching degrees, longer H-bond distances, and weaker interactions (Figure S7). MD simulation was further studied to evaluate the structural stability. As shown in Figure 4D,



biotin-modified MBMI-01c; the procedure for aptasensor preparation and sample detection was similar to the description in Section 4.4. Additionally, the response value should reach the plateau before the end of the association step; otherwise, the samples should be diluted. In addition, the buffer at the dissociation step should be consistent with the association step. Following the procedure, an independent detection was finished in 10 min.

Next, we assessed the properties of the aptasensor. CTX-MI in gradient concentrations of 0.5–100  $\mu\text{M}$  was measured, and the response values were fitted to the equation:  $y = (2.849 - 0.02272)/[1 + (x/155.6)^{-0.9271}] + 0.02272$  with an  $R^2$  of 0.9928 (Figure 5A), indicating the dose dependence of the response values. In addition, the linear range was 1–50  $\mu\text{M}$ , which was expressed by the equation:  $y = 0.0142x + 0.0792$  with an  $R^2$  value of 0.9981 (Figure 5B). Then, the standard deviation of the blank response was calculated based on ten independent detections. The limit of detection (LOD) and limit of quantification (LOQ) were 0.26 and 0.88 nM, respectively. Moreover, the standard solutions in the concentration of 5, 10, and 20  $\mu\text{M}$  were detected. The actual detection values were 5.48, 10.21, and 20.14  $\mu\text{M}$ , while the coefficients of variation (CV) were 3.25%, 2.45%, and 2% (Table 2), respectively, indicating that the aptasensor possessed good precision. Additionally, the anti-interference of the aptasensor was ensured by the specificity of MBMI-01c (Figure 3B) and the consistent buffer at the association and dissociation steps. To verify the influence of the matrix effect on the trueness, tap water with CTX-MI was tested, and the results are shown in Table 3. A good recovery percentage of 98.83% to 102.11% was obtained, while the CV values were 4.31%, 4.9%, and 2.21%, respectively. In summary, the aptasensor provided accurate and rapid quantification of CTX-MI at the range of 1–50  $\mu\text{M}$  with good precision, trueness, and repeatability.

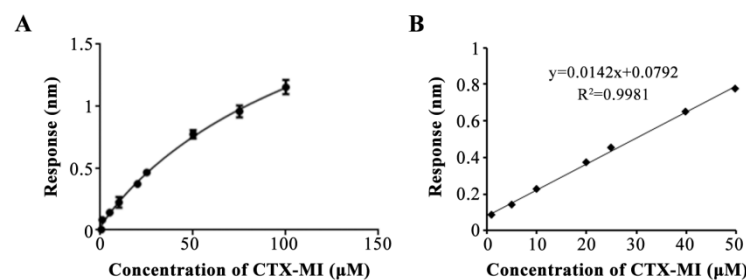


**Figure 5.** Curve fitting for the response value and CTX-MI concentration. (A) The calibration curve for CTX-MI from 0.5 to 100  $\mu\text{M}$ , a plot of the response value as a function of the CTX-MI concentration. The error bars represent standard deviations. (B) The linear range of the calibration curve for CTX-MI, a plot of the response as a function of the CTX-MI concentration from 1 to 50  $\mu\text{M}$ . All response values were detected by the BLI assay.

**Table 2.** Precision studies with different concentrations of CTX-MI ( $n = 3$ ).

CTX-MI ( $\mu\text{M}$ )	Detection Value ( $\mu\text{M}$ )	CV (%)
5	5.48	3.25
10	10.21	2.45
20	20.14	2.00

**Table 3.** Recovery studies of tap water with different concentrations of CTX-MI ( $n = 3$ ).

CTX-MI ( $\mu\text{M}$ )	Detection Value ( $\mu\text{M}$ )	CV (%)	Recovery (%)
10	10.47	4.31	102.11
25	24.71	4.90	98.83
50	50.53	2.21	101.06

At present, the methods for CTX-MI detection are extremely scarce; only high-performance liquid chromatography (HPLC) and matrix-assisted laser desorption/ionization mass spec-

trometry (MALDI-MS) have been reported [13,36]. The former is more widely used in the purification of synthetic CTX-MI [12,36]. The latter is widely used to identify peptides and proteins, which was proved feasible for CTX-MI detection according to Yasushi's report [13]. Although these methods are considered as the gold standard, the complicated process of sample preparation and detection, the extensive use of chemical reagents, and the expensive instruments limit their application scenarios. Although some results have shown that the detection time can be reduced to 40 min [13], these methods are still not conducive to mass screening and rapid detection. Although the detectable concentration range is comparable to previous methods [13], the BLI-based aptasensor has the following advantages: (1) A simplified process of sample preparation: the interference of the matrix on the trueness can be effectively eliminated because of the same buffer at the association and dissociation steps and the specific interaction between MBMI-01c and CTX-MI. Therefore, the process of sample extraction, purification, and enrichment can be simplified. (2) Rapid detection: the aptasensor preparation and sample detection can be completed in 10 min. In addition, the platform with eight channels can be used for simultaneous detection. (3) Low cost: the simplicity for the operator, the low-budget synthesis of aptamers, and the reproducible SSA sensors reduce the human and experimental costs. (4) Portability: the portable BLI platform makes in situ detection possible. Therefore, this aptasensor is more suitable for rapid and mass detection.

### 3. Conclusions

CTX-MI is the most toxic CTX, which poses a great threat to underwater operations [10]. This study was the first report of DNA aptamer selection and identification for CTX-MI. MBMI-01c, the aptamer for CTX-MI, was predicted to form a stable antiparallel GQ, which provided a groove to capture CTX-MI specifically. As confirmed by previous reports, the groove structure provides a binding platform for small molecules [31,37,38]. Subsequently, a BLI-based aptasensor was proposed, which has good accuracy and reproducibility in the concentration range of 1–50  $\mu$ M. The advantages of this aptasensor are the simple process for sample and sensor preparation, rapid detection with multiple channels, lower cost, good accuracy and repeatability, and anti-interference. Therefore, this aptasensor is an alternative tool to detect CTX-MI for rapid warning and poisoning diagnosis.

In recent years, a large number of aptamers for small molecules have been screened and applied in drug development [39,40], experimental research [16], and many other fields. According to the results of the MD simulation and BLI assay, we confirmed the good selectivity and affinity of MBMI-01c and the stability of the compound. Hence, as the novel recognition element, MBMI-01c can be applied for the clearance of CTX-MI, for the development of targeted antidotal agents, and as a probe for the research into toxicity mechanism and signal transmission.

More importantly, it is worth mentioning that the wider varieties of CTXs are also known as "the treasury of marine active molecules" because of their diverse biological activities [41]. Some of them have the potential for analgesia, antiseptics, anticonvulsion, and drug withdrawal, which are either currently used or have been tested in clinical trials [2,41–44]. Aptamers for these CTXs provide powerful tools for screening the medicinal species, identifying the active structures, and enriching the active components. Hence, scientific systematic and efficient methods for aptamer screening and characterizing are required. The programmed process we used, which was developed by MB-SELEX, HTS analysis, affinity detection, and computer simulation, was proved to be effective for aptamer screening and characterization for CTX-MI. The dominant sequences were effectively enriched while the low-affinity and nonspecific ssDNA were eliminated through progressively pressurized MB-SELEX. The variations in sequence diversity and frequency were intuitively characterized by HTS analysis, which could scientifically determine the dominant sequences. The programmed computer simulation, which was composed of 3D structure prediction, molecular docking, and MD simulation revealed detailed structural information and binding modes in the natural state. Associated with experimental affinity detection, the specific and efficient identification between the aptamers and targets was comprehensively described. More importantly, the contribution of each nucleotide toward recognition and affinity

was visually displayed, which was helpful for the subsequent modification and improvement of the aptamers. Hence, the programmed process is applicative to other CTXs.

## 4. Materials and Methods

### 4.1. Chemicals and Reagents

CTX-GI and CTX-MI were purchased from EFEBIO (Shanghai, China). OA, STX, and TTX were purchased from Taiwan Algal Science Inc. (Taiwan, China). DA was purchased from Sigma-Aldrich Co. LLC (Shanghai, China). All ssDNA oligonucleotides were synthesized and purified by Sangon Biotechnology Co. Ltd. (Shanghai, China). Qubit<sup>®</sup> ssDNA Assay Kits, Pierce<sup>™</sup> Quantitative Fluorometric Peptide Assay Kits, Dynabeads<sup>®</sup> M-270 Carboxylic Acid, and the relevant reagents were purchased from Thermo Fisher Scientific Inc. (Waltham, MA, USA). GoTaqHot<sup>®</sup> Start Colorless Master Mix was purchased from Promega Corporation (Madison, WI, USA). The QIAEX<sup>®</sup> II Gel Extraction Kit was obtained from Qiagen (Frankfurt, Germany). SSA sensors were purchased from ForteBio (Shanghai, China). The selection Buffer (SB) (0.9 mM CaCl<sub>2</sub>, 2.7 mM KCl, 1.5 mM KH<sub>2</sub>PO<sub>4</sub>, 0.6 mM MgCl<sub>2</sub>·6H<sub>2</sub>O, 0.1 M NaCl and 20 mM Na<sub>2</sub>HPO<sub>4</sub>, pH = 7.4) was purchased from Tiandz (Beijing, China). The SB was used for aptamer screening, the BLI assay, and the performance evaluation of the aptasensor.

### 4.2. Aptamers Selection In Vitro

#### 4.2.1. Preparation of MBs

According to the specification, CTX-MI or CTX-GI was coupled with the MBs for positive and counter selection, respectively. The N-terminal of CTX-MI and CTX-GI has a free amino group, which could form amide bonds with carboxyl on the surface of the Dynabeads<sup>®</sup> M-270 Carboxylic Acid. Briefly, CTX-GI or CTX-MI was dissolved in MES solution (25 mM, pH = 5.0) to 21 mM. Then, 50 mg of the EDC or NHS was dissolved in 1 mL MES solution. Next, 100 µL of MBs was washed twice with the MES solution and incubated with 50 µL of the EDC solution and 50 µL of the NHS solution at room temperature for 30 min to activate the superficial carboxyl groups. After removing the supernatant, 100 µL of the CTX-GI or CTX-MI solution was added and incubated for 1 h. After that, the supernatant was quantified using Pierce<sup>™</sup> Quantitative Fluorometric Peptide Assay Kits (Waltham, MA, USA) to calculate the efficiency of the immobilization. In order to quench the non-reacted activated carboxylic acid groups, the aforesaid MBs were incubated with 50 mM Tris (pH = 7.4) for 1 h. The coated MBs were collected, mixed with 100 µL SB, and stored at 4 °C. The blank MBs were also activated and quenched for counter selection. In this study, the concentrations of CTX-MI-MBs and CTX-GI-MBs were 14.7 µM and 16.2 µM, respectively.

#### 4.2.2. Random ssDNA Library and Primers

The sequences of the random ssDNA library and primers are shown in Table 4. An 80 nt random ssDNA library (Lib V<sub>1</sub>) was used, which consisted of a central region of 40 nt random nucleotides and 20 nt fixed nucleotides at both the 3' and 5' ends. The fixed nucleotides were primer binding sites for the amplification of the libraries, which were binding with F<sub>1</sub> and R<sub>1</sub>, respectively. In addition, the fixed regions at both ends can form a complementary pairing of 10 bp. The R<sub>1</sub> was designed with a poly adenine tail (A<sub>20</sub> = 20 nt A), which facilitated the separation of the two different-sized PCR products. The primers of F<sub>2</sub>–F<sub>6</sub> and R<sub>2</sub> were used to obtain the HTS samples.

**Table 4.** The sequence of the random ssDNA library and primers.

ID	Sequence (5' to 3')
Lib V <sub>1</sub>	ATTGGCACTCCACGCATAGG-N <sub>40</sub> - CCTATGCGTGCTACCGTGAA
F <sub>1</sub>	ATTGGCACTCCACGCATAGG
F <sub>2</sub>	AAAGCAATTGGCACTCCACGCATAGG
F <sub>3</sub>	AACGCCATTGGCACTCCACGCATAGG
F <sub>4</sub>	AAGGCGATTGGCACTCCACGCATAGG
F <sub>5</sub>	ACAGGAATTGGCACTCCACGCATAGG
F <sub>6</sub>	ACCGGCATTGGCACTCCACGCATAGG
R <sub>1</sub>	A <sub>20</sub> -Spacer <sub>18</sub> -TTCACGGTAGCACGCATAGG
R <sub>2</sub>	TTCACGGTAGCACGCATAGG

#### 4.2.3. Aptamer Selection by MB-SELEX

MB-SELEX was conducted according to the previous report [34]. The process is illustrated in Figure 1A, following the protocol detailed in Table S1. The ssDNA libraries were dissolved, denatured at 95 °C for 10 min, and cooled at 4 °C for 5 min to ensure the optimal structural conformation. The prepared libraries were added into the CTX-MI-MBs, filled with SB to 100 µL, and incubated at room temperature. During incubation, the ssDNA gradually formed specific tertiary structures. The sequences with affinity were immobilized on the CTX-MI-MBs by binding to CTX-MI. Then, the beads were incubated with SB to rinse the unbound ssDNA. The ssDNA combined with CTX-MI-MBs was eluted with 200 µL SB by heating at 95 °C for 30 min and quantified for the recovery ratio. Then, the eluted ssDNA was amplified by PCR, and the amplified ssDNA was prepared and collected from the PCR products for the next round. For the counter selection, the ssDNA libraries were incubated with counter beads (blank MBs or CTX-GI-MBs) to eliminate the nonspecific binding, and then the supernatants were recovered for the following positive selection.

#### 4.3. The Preparation of HTS Samples

After 12 rounds of selection, the enriched libraries of rounds 2, 4, 6, 9, and 12 were amplified with different forward primers (F<sub>2</sub>–F<sub>6</sub>) and the same reverse primer (R<sub>2</sub>) to carry different tags (Table 4). The PCR products in each pool were purified and mixed in equal quantities for the HTS analysis.

#### 4.4. The Determination of Affinity by BLI Assay

The BLI assay was conducted using the OctetRED K2 instrument (Sartorius, Shanghai, China) to determine the affinity parameter and response value. The procedure followed the previous report [34], and the details are shown in Figure S1. The procedure included five steps: baseline (1 min), loading (3 min), baseline-2 (1 min), association (2 min), and dissociation (3 min). Baseline and baseline-2 were balancing steps immersing with SB. The biotin-modified aptamers (2 µM) were immobilized on the SSA sensors at the loading step. After the baseline-2 step, the sensors were subjected to the association step, immersing with targets diluted in SB. Following the association step, the sensors were immersed in SB to estimate the dissociation. All the steps were performed at 25 °C. Toxin solutions were replaced with SB to exclude the effect caused by the buffer and sensors. The ForteBio Data Analysis 11.0 Software (Sartorius, Shanghai, China) was used to analyze the data. The K<sub>D</sub>, association constant (K<sub>on</sub>), and dissociation constant (K<sub>dis</sub>) were estimated to establish the binding affinity between the toxins and aptamers. The K<sub>D</sub> value was determined utilizing the 1:1 global fit model. According to the instrument instructions, the result is considered valid only if the K<sub>D</sub> error is at least an order of magnitude less than the K<sub>D</sub> value, X<sup>2</sup> < 3, and R<sup>2</sup> > 0.8. Otherwise, the result is a false-positive and is considered a non-affinity.

#### 4.5. Computer Simulation

##### 4.5.1. Three-Dimensional Structure Prediction of MBMI-01c

Firstly, the sequence of MBMI-01c was submitted to the QGRS Mapper web server (<http://bioinformatics.ramapo.edu/QGRS/analyze.php>) (accessed on 28 June 2022) to predict the composition and distribution of the QGRS [45]. The G-score was output according to the possibility of forming stable GQ. We further predicted all possible 3D structures with the highest Gscore by the G-Quadruplex module of the 3D-Nus web server (<https://www.iith.ac.in/3dnus/Quadruplex.html>) (accessed on 1 July 2022) [46]. Based on the output GQ-core models, the full-length 3D structures were constructed by extending and linking the residual nucleotides outside the core fragment using Discovery studio (Ver.4.6). For the conformational stability of the core fragment, Mg<sup>2+</sup> ions were placed in the center of each GQ-core, and then energy minimization was carried out to remove possible geometric deficiencies using the CHARMM force fields of Discovery studio [47]. Subsequently, the thermostable model, which was treated as the natural conformation, was obtained by TdMD simulation [31].

##### 4.5.2. Molecular Docking

The structures of CTX-MI, CTX-GI, STX, and OA (.sdf) were downloaded from the NCBI Pubchem Compound database (<https://www.ncbi.nlm.nih.gov/pccompound>) (accessed on 9 July 2022). The structure of MBMI-01c was optimized by cleaning geometry using Discovery studio and saved as a PDB file. Then, semi-flexible docking was performed using Hex (Ver.8.0). For each docking system, the receptor and ligand were permitted to rotate 180°, and the size of the docking box was set to 10 Å.

##### 4.5.3. MD Simulation

MD simulation was performed by GROMACS with the SPC water model. In each system, the model of the aptamer was placed in the center of a water box (20 Å<sup>3</sup>); the solvent layer between the edge of the box and the solute surface was set to 10 Å; Mg<sup>2+</sup> and Cl<sup>−</sup> ions were randomly placed by replacing water molecules to neutralize the system. The parameter file was configured according to the AMBER99SB-ILDN force field [48]. The LINCS algorithm was employed to constrain all covalent bonds for hydrogen, and a time-step of 1.0 fs was used. The remote electrostatic interaction was processed using the Particle-Mesh-Ewald (PME) method [49], and the cut-off distance of the electrostatic and van der Waals force was set to 4 Å. When dealing with the solvated system, the minimization of the steepest descent and the minimization of the conjugate gradient were 2000 cycles; all atoms were set to 50 kcal/(mol·Å<sup>2</sup>); the solvent molecules and hydrogen atoms were set to move freely. In the warming phase, the Langevin dynamic simulation algorithm was used to heat the system from 0 K to 300 K in 50 ps and to balance with 1 atm fixed pressure for 400 ps [50]. In the heating phase, the weak constraint of 10 kcal/(mol·Å<sup>2</sup>) was applied to all atoms, and the Velocity rescaling [51] algorithm was used to group the aptamers, toxins, and aptamer-toxin complexes. Each periodic boundary dynamics simulation was performed at a controlled temperature of 300 K and a controlled pressure of 1 atm. The variation curves of the RMSD values were derived after a 100 ns simulation to judge the stability of the conformation.

#### 4.6. Performance Evaluation of the BLI Aptasensor

To characterize the practicability of this BLI aptasensor, the linear range, LOD, LOQ, precision, specificity, accuracy, and feasibility were tested according to the previous reports [20,52]. The linear range was measured by testing the CTX-MI standards in the concentration range of 0.5–100 µM. The relation between the response value and the CTX-MI concentration was described by the sigmoidal logistic four-parameter equation, as follows:

$$y = (R_{\max} - R_{\min}) / [1 + (x/EC_{50})^b] + R_{\min} \quad (1)$$

where  $R_{\max}$  and  $R_{\min}$  are the maximum and minimum response values, respectively.  $EC_{50}$  represents the concentration at which the response value reaches half of the maximum response value, and  $b$  is the slope of the curve. The linear range was obtained according to the aforesaid curve and was considered satisfactory if  $R^2 > 0.99$ . The LOD and LOQ were determined by testing the blank groups ( $n = 10$ ) according to the following equations:

$$LOD = 3S/b \quad (2)$$

$$LOQ = 10S/b \quad (3)$$

where  $S$  is the standard deviation of the response value, and  $b$  is the slope of the linear regression equation. The precision was estimated with the CV by testing the CTX-MI standards in the concentrations of 5, 10, and 20  $\mu\text{M}$  ( $n = 3$ ). The accuracy and feasibility were estimated by the standard recovery rate in tap water, and the concentrations of CTX-MI were 10, 20, and 25  $\mu\text{M}$  ( $n = 3$ ).

#### 4.7. Treatment of Real Samples

Tap water samples with different concentrations of CTX-MI standards were prepared according to Ouyang's report [34]. Briefly, 1 mL of tap water spiked with CTX-MI standards was evaporated, resuspended with 1 mL SB, and filtered through the 0.45  $\mu\text{m}$  filters.

#### 4.8. Statistical Analysis

Statistical analysis was performed by Microsoft Excel 2010 or GraphPad Prism 6.0. The data were subjected to analysis by Student's  $t$ -test using SPSS version 22.0. The mean differences were considered significant at  $p < 0.05$ .

**Supplementary Materials:** The following supporting information can be downloaded at: <https://www.mdpi.com/article/10.3390/toxins14100706/s1>. Table S1: MB-SELEX conditions for aptamer screening. Table S2: The information of the top 10 sequences. Table S3: The information of the candidate aptamers. Table S4: Affinity constants between the CTX-MI and candidate aptamers. Table S5: The QGRS prediction of MBMI-01c. Table S6: The information of the mutational sequences. Table S7: The QGRS prediction of the mutational sequences. Figure S1: The procedure of the BLI assay. Figure S2: The information of the alternative aptamers. (A) Multiple sequence alignment by Clustal X 2.1. The full length of the sequences (80 nt) was used here. (B) The N-J tree constructing by Mega 7. These sequences were grouped into four families (I-IV). Figure S3: The candidate full-length models of each possible GQ-core. Figure S4: RMSD vs. simulation time in the constant-temperature phase. Figure S5: RMSD vs. simulation time in the heating phase. Figure S6: RMSD vs. simulation in the second round of TdMD simulation. (A) The results in the constant-temperature phase. (B) The results in the heating phase. Figure S7: Three-dimensional view of the interactions between MBMI-01c and the ligands (A. CTX-GI; B. OA; C. STX). The hydrogen bond between the docking site of MBMI-01c and the ligand is depicted by a yellow dashed line, and the distance is marked next to the dashed line.

**Author Contributions:** Conceptualization, H.G. and L.W.; Data curation, Y.G. and M.S.; Formal analysis, H.G.; Funding acquisition, L.W.; Investigation, H.G.; Methodology, H.G. and X.Z.; Project administration, L.W. and B.J.; Software, B.D.; Supervision, B.J.; Validation, L.Z. and C.Y.; Writing—original draft, H.G.; Writing—review and editing, B.D., B.Z. and H.C. All authors have read and agreed to the published version of the manuscript.

**Funding:** This research was funded by Nation Natural Science Foundation of China (No. 82173732), and National Key R&D Program of China (No. 2019YFC0312603).

**Institutional Review Board Statement:** Not applicable.

**Informed Consent Statement:** Not applicable.

**Data Availability Statement:** Not applicable.

**Conflicts of Interest:** The authors declare no conflict of interest.

## Abbreviations

Abbreviation	Full Name
BLI	biolayer interferometry
CTX-GI	$\alpha$ -conotoxin GI
CTX-GI-MBs	CTX-GI coated MBs
CTX-MI	$\alpha$ -conotoxin MI
CTX-MI-MBs	CTX-MI coated MBs
CTXs	conotoxins
CV	coefficient of variation
DA	domoic acid
GQ	G-quadruplet
HPLC	high-performance liquid chromatography
HTS	high-throughput sequencing
LOD	limit of detection
LOQ	limit of quantification
MALDI	matrix-assisted laser desorption/ionization
MB	magnetic beads
MD	molecular dynamics
MS	mass spectrometry
N-J tree	neighbor-joining tree
OA	okadaic acid
PME	Particle-Mesh-Ewald
QGRS prediction	G-rich sequences prediction
RMSD	root mean square deviation
SB	selection buffer
SELEX	systematic evolution of ligands by exponential enrichment
SSA	super streptavidin
STX	saxitoxin
TdMD	temperature-dependent molecular dynamics simulation
TTX	tetrodotoxin
3D	three-dimensional

## References

- Gao, B.; Peng, C.; Yang, J.; Yi, Y.; Zhang, J.; Shi, Q. Cone snails: A big store of conotoxins for novel drug discovery. *Toxins* **2017**, *9*, 397. [[CrossRef](#)]
- Becker, S.; Terlau, H. Toxins from cone snails: Properties, applications and biotechnological production. *Appl. Microbiol. Biotechnol.* **2008**, *79*, 1–9. [[CrossRef](#)] [[PubMed](#)]
- Peng, C.; Yao, G.; Gao, B.M.; Fan, C.X.; Bian, C.; Wang, J.; Cao, Y.; Wen, B.; Zhu, Y.; Ruan, Z.; et al. High-throughput identification of novel conotoxins from the Chinese tubular cone snail (*Conus betulinus*) by multi-transcriptome sequencing. *Gigascience* **2016**, *5*, 17–30. [[CrossRef](#)] [[PubMed](#)]
- Himaya, S.; Jin, A.H.; Hamilton, B.; Rai, S.K.; Alewood, P.; Lewis, R.J. Venom duct origins of prey capture and defensive conotoxins in piscivorous *Conus striatus*. *Sci. Rep.* **2021**, *11*, 13282–13295. [[CrossRef](#)]
- Robinson, S.D.; Norton, R.S. Conotoxin gene superfamilies. *Mar. Drugs* **2014**, *12*, 6058–6101. [[CrossRef](#)] [[PubMed](#)]
- Jin, A.H.; Muttenthaler, M.; Dutertre, S.; Himaya, S.; Kaas, Q.; Craik, D.J.; Lewis, R.J.; Alewood, P.F. Conotoxins: Chemistry and biology. *Chem. Rev.* **2019**, *119*, 11510–11549. [[CrossRef](#)]
- Gowd, K.H.; Sabareesh, V.; Sudarslal, S.; Iengar, P.; Franklin, B.; Fernando, A.; Dewan, K.; Ramaswami, M.; Sarma, S.P.; Sikdar, S.; et al. Novel peptides of therapeutic promise from Indian *Conidae*. *Ann. N. Y. Acad. Sci.* **2005**, *1056*, 462–473. [[CrossRef](#)]
- Kohn, A.J.; Saunders, P.R.; Wiener, S. Preliminary studies on the venom of the marine snail *Conus*. *Ann. N. Y. Acad. Sci.* **1960**, *90*, 706–725. [[CrossRef](#)]
- Rice, R.D.; Halstead, B.W. Report of fatal cone shell sting by *Conus geographus* Linnaeus. *Toxicon* **1968**, *5*, 223–224. [[CrossRef](#)]
- Endean, R.; Rudkin, C. Further studies of the venoms of conidae. *Toxicon* **1965**, *2*, 225–249. [[CrossRef](#)]
- Gray, W.R.; Rivier, J.E.; Galyean, R.; Cruz, L.J.; Olivera, B.M. Conotoxin MI. Disulfide bonding and conformational states. *J. Biol. Chem.* **1983**, *258*, 12247–12251. [[CrossRef](#)]
- Zhang, M.; Yu, S.; Zhang, X.; Huang, Q.; Huang, Y.; Luo, M.; Wei, Y.; Chen, W.; Chen, Z.; Zhou, X.; et al. A new protein-coupled antigen of alpha-conotoxin MI displays high immunogenicity and can produce antiserum with high detoxification activity. *Toxicon* **2022**, *208*, 53–61. [[CrossRef](#)] [[PubMed](#)]

13. Shigeri, Y.; Inazumi, S.; Hagihara, Y.; Yasuda, A.; Kawasaki, H.; Arakawa, R.; Nakata, M. Desorption/ionization efficiency of peptides containing disulfide bonds in matrix-assisted laser desorption/ionization mass spectrometry. *Anal. Sci.* **2012**, *28*, 295–299. [[CrossRef](#)]
14. Dionysiou, D. Overview: Harmful algal blooms and natural toxins in fresh and marine waters—Exposure, occurrence, detection, toxicity, control, management and policy. *Toxicon* **2010**, *55*, 907–908. [[CrossRef](#)] [[PubMed](#)]
15. Ellington, A.D.; Szostak, J.W. In vitro selection of RNA molecules that bind specific ligands. *Nature* **1990**, *346*, 818–822. [[CrossRef](#)] [[PubMed](#)]
16. Zhang, Y.; Lai, B.S.; Juhas, M. Recent advances in aptamer discovery and applications. *Molecules* **2019**, *24*, 941. [[CrossRef](#)]
17. Ye, W.; Liu, T.; Zhang, W.; Zhu, M.; Liu, Z.; Kong, Y.; Liu, S. Marine toxins detection by biosensors based on aptamers. *Toxins* **2019**, *12*, 1. [[CrossRef](#)] [[PubMed](#)]
18. Tuerk, C.; Gold, L. Systematic evolution of ligands by exponential enrichment: RNA ligands to bacteriophage T4 DNA polymerase. *Science* **1990**, *249*, 505–510. [[CrossRef](#)]
19. Jayasena, S.D. Aptamers: An emerging class of molecules that rival antibodies in diagnostics. *Clin. Chem.* **1999**, *45*, 1628–1650. [[CrossRef](#)]
20. Gao, S.; Hu, B.; Zheng, X.; Cao, Y.; Liu, D.; Sun, M.; Jiao, B.; Wang, L. Gonyautoxin 1/4 aptamers with high-affinity and high-specificity: From efficient selection to aptasensor application. *Biosens. Bioelectron.* **2016**, *79*, 938–944. [[CrossRef](#)]
21. Kaur, H.; Shorie, M.; Sabherwal, P. Bilayer interferometry-SELEX for Shiga toxin antigenic-peptide aptamers & detection via chitosan-WSe2 aptasensor. *Biosens. Bioelectron.* **2020**, *167*, 112498–112522. [[CrossRef](#)] [[PubMed](#)]
22. Gupta, A.; Anand, A.; Jain, N.; Goswami, S.; Anantharaj, A.; Patil, S.; Singh, R.; Kumar, A.; Shrivastava, T.; Bhatnagar, S.; et al. A novel G-quadruplex aptamer-based spike trimeric antigen test for the detection of SARS-CoV-2. *Mol. Ther.-Nucleic Acids* **2021**, *26*, 321–332. [[CrossRef](#)] [[PubMed](#)]
23. Shkempi, X.; Skouridou, V.; Svobodova, M.; Leonardo, S.; Bashammakh, A.S.; Alyoubi, A.O.; Campàs, M.; O’ Sullivan, C.K. Hybrid antibody—Aptamer assay for detection of tetrodotoxin in pufferfish. *Anal. Chem.* **2021**, *93*, 14810–14819. [[CrossRef](#)] [[PubMed](#)]
24. Cruz, L.J.; Gray, W.R.; Olivera, B.M. Purification and properties of a myotoxin from *Conus geographus* venom. *Arch. Biochem. Biophys.* **1978**, *190*, 539–548. [[CrossRef](#)]
25. Mergny, J.L.; Phan, A.T.; Lacroix, L. Following G-quartet formation by UV-spectroscopy. *FEBS Lett.* **1998**, *435*, 74–78. [[CrossRef](#)]
26. Patel, D.J.; Phan, A.T.; Kuryavyy, V. Human telomere, oncogenic promoter and 5'-UTR G-quadruplexes: Diverse higher order DNA and RNA targets for cancer therapeutics. *Nucleic Acids Res.* **2007**, *35*, 7429–7455. [[CrossRef](#)]
27. Huppert, J.L. Four-stranded DNA: Cancer, gene regulation and drug development. *Philos. Trans. R. Soc. A Math. Phys. Eng. Sci.* **2007**, *365*, 2969–2984. [[CrossRef](#)]
28. Oganessian, L.; Bryan, T.M. Physiological relevance of telomeric G-quadruplex formation: A potential drug target. *Bioessays* **2007**, *29*, 155–165. [[CrossRef](#)]
29. Wang, K.Y.; McCurdy, S.; Shea, R.G.; Swaminathan, S.; Bolton, P.H. A DNA aptamer which binds to and inhibits thrombin exhibits a new structural motif for DNA. *Biochemistry* **1993**, *32*, 1899–1904. [[CrossRef](#)]
30. Marsh, T.C.; Vesenska, J.; Henderson, E. A new DNA nanostructure, the G-wire, imaged by scanning probe microscopy. *Nucleic Acids Res.* **1995**, *23*, 696–700. [[CrossRef](#)]
31. Song, M.; Li, G.; Zhang, Q.; Liu, J.; Huang, Q. De novo post-SELEX optimization of a G-quadruplex DNA aptamer binding to marine toxin gonyautoxin 1/4. *Comput. Struct. Biotechnol. J.* **2020**, *18*, 3425–3433. [[CrossRef](#)] [[PubMed](#)]
32. Concepcion, J.; Witte, K.; Wartchow, C.; Choo, S.; Yao, D.; Persson, H.; Wei, J.; Li, P.; Heidecker, B.; Ma, W.; et al. Label-free detection of biomolecular interactions using BioLayer interferometry for kinetic characterization. *Comb. Chem. High Throughput Screen.* **2009**, *12*, 791–800. [[CrossRef](#)] [[PubMed](#)]
33. Sultana, A.; Lee, J.E. Measuring protein-protein and protein-nucleic acid interactions by bilayer interferometry. *Curr. Protoc. Protein Sci.* **2015**, *79*, 19–25. [[CrossRef](#)] [[PubMed](#)]
34. Ouyang, S.; Hu, B.; Zhou, R.; Liu, D.; Peng, D.; Li, Z.; Li, Z.; Jiao, B.; Wang, L. Rapid and sensitive detection of nodularin-R in water by a label-free BLI aptasensor. *Analyst* **2018**, *143*, 4316–4322. [[CrossRef](#)]
35. Zhang, X.; Gao, Y.; Deng, B.; Hu, B.; Zhao, L.; Guo, H.; Yang, C.; Ma, Z.; Sun, M.; Jiao, B.; et al. Selection, characterization, and optimization of DNA aptamers against challenging marine biotoxin gymnodimine-a for biosensing application. *Toxins* **2022**, *14*, 195. [[CrossRef](#)]
36. Bren, N.; Sine, S.M. Hydrophobic pairwise interactions stabilize alpha-conotoxin MI in the muscle acetylcholine receptor binding site. *J. Biol. Chem.* **2000**, *275*, 12692–12700. [[CrossRef](#)]
37. Wong, H.M.; Stegle, O.; Rodgers, S.; Huppert, J.L. A toolbox for predicting g-quadruplex formation and stability. *J. Nucleic Acids* **2010**, *2010*, 564946. [[CrossRef](#)]
38. Hu, B.; Zhou, R.; Li, Z.; Ouyang, S.; Li, Z.; Hu, W.; Wang, L.; Jiao, B. Study of the binding mechanism of aptamer to palytoxin by docking and molecular simulation. *Sci. Rep.* **2019**, *9*, 15494–15504. [[CrossRef](#)]
39. Mufhandu, H.T.; Gray, E.S.; Madiga, M.C.; Tumba, N.; Alexandre, K.B.; Khoza, T.; Wibmer, C.K.; Moore, P.L.; Morris, L.; Khati, M. UCLA1, a synthetic derivative of a gp120 RNA aptamer, inhibits entry of human immunodeficiency virus type 1 subtype C. *J. Virol.* **2012**, *86*, 4989–4999. [[CrossRef](#)]

40. Hoellenriegel, J.; Zboralski, D.; Maasch, C.; Rosin, N.Y.; Wierda, W.G.; Keating, M.J.; Kruschinski, A.; Burger, J.A. The spiegelmer NOX-A12, a novel CXCL12 inhibitor, interferes with chronic lymphocytic leukemia cell motility and causes chemosensitization. *Blood* **2014**, *123*, 1032–1039. [[CrossRef](#)]
41. Akondi, K.B.; Muttenthaler, M.; Dutertre, S.; Kaas, Q.; Craik, D.J.; Lewis, R.J.; Alewood, P.F. Discovery, synthesis, and structure–activity relationships of conotoxins. *Chem. Rev.* **2014**, *114*, 5815–5847. [[CrossRef](#)] [[PubMed](#)]
42. Lewis, R.J.; Nielsen, K.J.; Craik, D.J.; Loughnan, M.L.; Adams, D.A.; Sharpe, I.A.; Luchian, T.; Adams, D.J.; Bond, T.; Thomas, L.; et al. Novel omega-conotoxins from *Conus catus* discriminate among neuronal calcium channel subtypes. *J. Biol. Chem.* **2000**, *275*, 35335–35344. [[CrossRef](#)] [[PubMed](#)]
43. Livett, B.G.; Gayler, K.R.; Khalil, Z. Drugs from the sea: Conopeptides as potential therapeutics. *Curr. Med. Chem.* **2004**, *11*, 1715–1723. [[CrossRef](#)] [[PubMed](#)]
44. Livett, B.G.; Sandall, D.W.; Keays, D.; Down, J.; Gayler, K.R.; Satkunathan, N.; Khalil, Z. Therapeutic applications of conotoxins that target the neuronal nicotinic acetylcholine receptor. *Toxicon* **2006**, *48*, 810–829. [[CrossRef](#)] [[PubMed](#)]
45. Kikin, O.; D’Antonio, L.; Bagga, P.S. QGRS Mapper: A web-based server for predicting G-quadruplexes in nucleotide sequences. *Nucleic Acids Res.* **2006**, *34*, 676–682. [[CrossRef](#)] [[PubMed](#)]
46. Patro, L.; Kumar, A.; Kolimi, N.; Rathinavelan, T. 3D-NuS: A web server for automated modeling and visualization of non-canonical 3-dimensional nucleic acid structures. *J. Mol. Biol.* **2017**, *429*, 2438–2448. [[CrossRef](#)] [[PubMed](#)]
47. Brooks, B.R.; Bruccoleri, R.E.; Olafson, B.D.; States, D.J.; Karplus, M. CHARMM: A program for macromolecular energy, minimization, and dynamics calculations. *J. Comput. Chem.* **2010**, *4*, 187–217. [[CrossRef](#)]
48. Piana, S.; Klepeis, J.L.; Shaw, D.E. Assessing the accuracy of physical models used in protein-folding simulations: Quantitative evidence from long molecular dynamics simulations. *Curr. Opin. Struct. Biol.* **2014**, *24*, 98–105. [[CrossRef](#)]
49. Case, D.A.; Cheatham, T.R.; Darden, T.; Gohlke, H.; Luo, R.; Merz, K.J.; Onufriev, A.; Simmerling, C.; Wang, B.; Woods, R.J. The Amber biomolecular simulation programs. *J. Comput. Chem.* **2005**, *26*, 1668–1688. [[CrossRef](#)] [[PubMed](#)]
50. Henrik, G.P. Accuracy and efficiency of the particle mesh Ewald method. *J. Chem. Phys.* **1995**, *103*, 3668–3679. [[CrossRef](#)]
51. Pastor, R.W.; Brooks, B.R.; Szabo, A. An analysis of the accuracy of Langevin and molecular dynamics algorithms. *Mol. Phys.* **1988**, *65*, 1409–1419. [[CrossRef](#)]
52. Shrivastava, A. Methods for the determination of limit of detection and limit of quantitation of the analytical methods. *Drug Discov. Ther.* **2011**, *2*, 21–25. [[CrossRef](#)]